Exploring the hydraulic failure hypothesis on esca leaf symptom formation

Bortolami, G.; Gambetta, G.A.; Delzon, S.; Lamarque, L.J.; Pouzoulet, J.; Badel, E.; ... ; Delmas, C.E.L.

Exploring the Hydraulic Failure Hypothesis of Esca Leaf Symptom Formation[1][OPEN]

Giovanni Bortolami,[a] Gregory A. Gambetta,[b] Sylvain Delzon,[c] Laurent J. Lamarque,[c] Jérôme Pouzoulet,[b] Eric Badel,[d] Régis Burlett,[c] Guillaume Charrier,[d] Hervé Cochard,[d] Silvina Dayer,[b] Steven Jansen,[e] Andrew King,[f] Pascal Lecomte,[a] Frederic Lens,[g] José M. Torres-Ruiz,[d] and Chloé E.L. Delmas[a,2,3]

[a]SAVE, INRA, BSA, ISVV, 33882 Villenave d'Ornon, France
[b]EGFV, Bordeaux-Sciences Agro, INRA, Université Bordeaux, ISVV, 33882 Villenave d'Ornon, France
[c]BIOGECO, INRA, Université Bordeaux, 33610 Cestas, France
[d]Université Clermont Auvergne, INRA, PIAF, F-63000 Clermont-Ferrand, France
[e]Institute of Systematic Botany and Ecology, Ulm University, D-89081 Ulm, Germany
[f]Synchrotron SOLEIL, L'Orme de Merisiers, Saint Aubin-BP48, 91192 Gif-sur-Yvette cedex, France
[g]Naturalis Biodiversity Center, Leiden University, 2300RA Leiden, The Netherlands

ORCID IDs: 0000-0001-7528-9644 (G.B.); 0000-0002-8838-5050 (G.A.G.); 0000-0003-3442-1711 (S.D.); 0000-0002-1430-5193 (L.J.L.); 0000-0001-8589-3474 (J.P.); 0000-0003-2282-7554 (E.B.); 0000-0001-8289-5757 (R.B.); 0000-0001-8722-8822 (G.C.); 0000-0002-2727-7072 (H.C.); 0000-0002-4476-5334 (S.J.); 0000-0002-0479-0295 (P.L.); 0000-0002-5001-0149 (F.L.); 0000-0003-1367-7056 (J.M.T.-R.); 0000-0003-3568-605X (C.E.L.D.).

Vascular pathogens cause disease in a large spectrum of perennial plants, with leaf scorch being one of the most conspicuous symptoms. Esca in grapevine (*Vitis vinifera*) is a vascular disease with huge negative effects on grape yield and the wine industry. One prominent hypothesis suggests that vascular disease leaf scorch is caused by fungal pathogen-derived elicitors and toxins. Another hypothesis suggests that leaf scorch is caused by hydraulic failure due to air embolism, the pathogen itself, and/or plant-derived tyloses and gels. In this study, we transplanted mature, naturally infected esca symptomatic vines from the field into pots, allowing us to explore xylem integrity in leaves (i.e. leaf midveins and petioles) using synchrotron-based in vivo x-ray microcomputed tomography and light microscopy. Our results demonstrated that symptomatic leaves are not associated with air embolism. In contrast, symptomatic leaves presented significantly more nonfunctional vessels resulting from the presence of nongaseous embolisms (i.e. tyloses and gels) than control leaves, but there was no significant correlation with disease severity. Using quantitative PCR, we determined that two vascular pathogen species associated with esca necrosis in the trunk were not found in leaves where occlusions were observed. Together, these results demonstrate that symptom development is associated with the disruption of vessel integrity and suggest that symptoms are elicited at a distance from the trunk where fungal infections occur. These findings open new perspectives on esca symptom expression where the hydraulic failure and elicitor/toxin hypotheses are not necessarily mutually exclusive.

Maintaining the integrity of the plant vascular system is crucial for plant health and productivity. Xylem tissue transports water and mineral nutrients and forms a complex reticulate network of many interconnected vessels (Zimmermann, 1983). This complex network of vessels hosts a large breadth of endophytic microorganisms, most of which live harmlessly within the plant (Fisher et al., 1993; Oses et al., 2008; Qi et al., 2012). However, some organisms in the vessel lumina can be (or become) pathogenic, and this class of pathogens is referred to as vascular pathogens (Pearce, 1996). Vascular pathogens are highly diverse, and their pathologies depend on the specific pathogen-host interaction. They cause diseases in a wide taxonomic range of plant species.

Plant vascular disorders are sometimes identified by conspicuous leaf scorch symptoms, which are strikingly similar and typically begin with necrosis at the leaf margin. The exact mechanisms driving these leaf symptoms remain largely unknown, and there are two long-standing and unresolved working hypotheses (Fradin and Thomma, 2006; Surico et al., 2006; McElrone et al., 2010; Sun et al., 2013; Yadeta and Thomma, 2013; Oliva et al., 2014; Pouzoulet et al., 2014). The first hypothesis proposes that symptoms result from the transport of pathogen-derived elicitors or toxins through the transpiration stream. The second proposes that symptoms result from hydraulic failure resulting from any combination of air embolism, occlusion of xylem vessels from the pathogen itself, and/or occlusion of xylem vessels by plant-derived tyloses and gels.

Esca disease in grapevine (*Vitis vinifera*) is one case where the conflict between these two hypotheses of leaf symptom formation remains unresolved (Surico et al., 2006; Pouzoulet et al., 2014). Esca is characterized by three main symptoms: leaf scorch, trunk necrosis, and a colored stripe along the vasculature (Lecomte et al., 2012). Esca belongs to a complex of diseases referred to as grapevine trunk diseases, which cause defoliation,

berry loss, and vine death (Bertsch et al., 2013; Mondello et al., 2018; Gramaje et al., 2018). This disease has been recognized for thousands of years and has been increasingly the focus of research over the past two decades, as it is believed to be one of the main causes of grape production decline, especially in Europe, the United States (California), and South Africa (Cloete et al., 2015; Guerin-Dubrana et al., 2019). The fungi most strongly associated with esca wood necrosis in the trunk have been identified (Larignon and Dubos, 1997; Mugnai et al., 1999; Fischer 2006; White et al., 2011; Bruez et al., 2014; Morales-Cruz et al., 2018). While the disease was formerly associated with the presence of soft rot (caused by basidiomycetes such as *Fomitiporia mediterranea*), studies have identified two vascular pathogens, *Phaeomoniella chlamydospora* and *Phaeoacremonium minimum*, which are detected in trunk necrotic tissues of esca symptomatic vines (Feliciano et al., 2004; Massonnet et al., 2018; Morales-Cruz et al., 2018). Esca leaf symptoms are only observed on mature vines (more than 7 years old) in the field (Mondello et al., 2018) and cannot be reliably reproduced by inoculating vines with the causal fungi (Surico et al., 2006; Bruno et al., 2007), despite testing various methodologies (Reis et al., 2019). This suggests that leaf scorch symptoms are the result of complex host-pathogen-environment interactions (Fischer and Peighami-Ashnaei, 2019). Neither the elicitor/toxin nor the hydraulic failure hypothesis of esca pathogenesis has been experimentally confirmed. It is generally accepted that the fungi responsible for esca wood necrosis are not present in leaves and that leaf symptoms are a consequence of fungal activities in the perennial organs (i.e. trunk). However, to our knowledge, leaves and current-year stems have never been investigated in detail to see if the key pathogens detected in necrotic regions of the perennial wood also occur in these organs.

In this study, we created an experimental system for the study of esca disease by transplanting mature, naturally infected esca symptomatic vines from the field into large pots. This allowed us to test the hydraulic failure hypothesis by exploring vessel integrity (presence of air embolism, occlusion, and the pathogens themselves) in leaves using noninvasive, in vivo imaging via x-ray microcomputed tomography (microCT), light microscopy, and quantitative PCR (qPCR). MicroCT avoids artifacts caused by traditional invasive techniques (Torres-Ruiz et al., 2015) and allows for the visualization of vessel content and functionality in esca symptomatic leaf petioles and midribs. We assessed the presence of two of the main pathogens associated with esca, *P. chlamydospora* and *P. minimum*, using qPCR in annual stems, leaves, and multiyear branches. These two species are tracheomycotic agents and could thus, in theory, disperse systemically via the sap flow from the trunk (Pouzoulet et al., 2014). This study provides new perspectives regarding the pathogenesis of esca leaf symptom formation.

RESULTS

Vessel Occlusion and the Percentage Loss of Conductivity in Symptomatic and Asymptomatic Leaves

Midrib and petiole vascular bundles of symptomatic and asymptomatic leaves were imaged in three dimensions using microCT (Fig. 1; Supplemental Figs. S1 and S2). These analyses allowed for the identification of embolized and occluded xylem vessels and the quantification of the percentage loss of theoretical hydraulic conductivity (PLC). The level of native air embolism was very low, ranging from 2.8% to 9.7%, for both asymptomatic and symptomatic midribs (Fig. 1, A and C) and petioles (Supplemental Fig. S1, A and D). There were no significant differences in the levels of native air embolism between symptomatic and asymptomatic leaves in petioles or midribs (Table 1; Fig. 2).

After exposing the xylem vessels to air by cutting the leaf or petiole just above (<2 mm) the scanned area, some proportion of vessels did not embolize immediately and apparently remained water filled (Fig. 1, B and D; Supplemental Figs. S1, B and E, red arrows, S2, C and D). These vessels were considered occluded. The average PLC in asymptomatic midribs due to occluded vessels was 12.4% ± 3.2%, while symptomatic midribs showed significantly higher values, 68.8% ± 6.4% (Table 1; Fig. 3). This is also the case for petioles, where asymptomatic leaves exhibited a PLC of only 1.9% ± 1.8%, while PLC in symptomatic leaves was 55.3% ± 9% (Table 1; Fig. 3). Detailed information on the contributions of different kinds of vessels to the theoretical hydraulic conductivity is presented in Supplemental Table S1.

[1]This work was supported by the French Ministry of Agriculture, Agrifood, and Forestry (FranceAgriMer and CNIV) within the PHYSIOPATH project (program Plan National Dépérissement du Vignoble, 22001150-1506), the Agence Nationale de la Recherche Cluster of Excellence COTE (ANR-10-LABX-45, within the VIVALDI and DEFI projects) and program Investments for the Future (ANR-10-EQPX-16, XYLOFOREST), and the AgreenSkills Fellowship program, which received funding from the European Union's Seventh Framework Program (FP7 26719-688 to G.C.).

[2]Author for contact: chloe.delmas@inra.fr.

[3]Senior author.

The author responsible for distribution of materials integral to the findings presented in this article in accordance with the policy described in the Instructions for Authors (www.plantphysiol.org) is: Chloé E.L. Delmas (chloe.delmas@inra.fr).

C.E.L.D., G.A.G., G.B., and S.De. designed experiments and analyzed the data; A.K., E.B., F.L., G.A.G., G.B., G.C., H.C., J.M.T.-R., L.J.L., R.B., S.Da., S.De., and S.J. participated in synchrotron campaigns; C.E.L.D. and G.B. conducted the histological observation; P.L. provided data on disease history of the plants used in this study; J.P. conducted the pathogen detection; G.B. analyzed the microCT images; C.E.L.D., G.A.G., and G.B. wrote the article; all authors edited and agreed on the last version of the article.

[OPEN]Articles can be viewed without a subscription.

www.plantphysiol.org/cgi/doi/10.1104/pp.19.00591

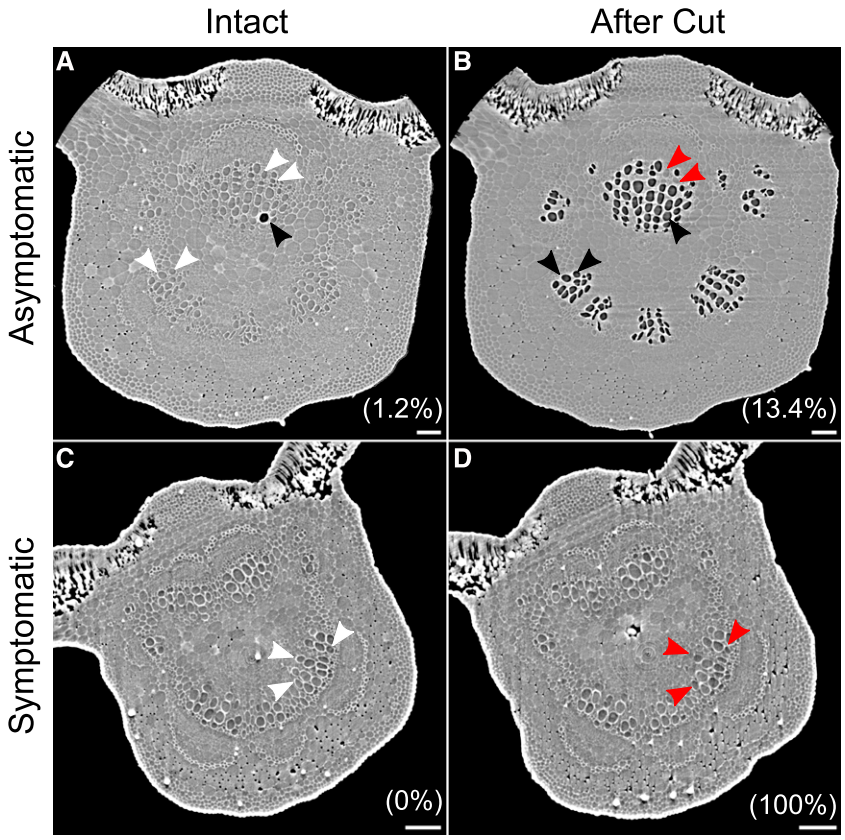

Figure 1. Two-dimensional reconstructions of cross sections from microCT volumes of grapevine leaves. Esca asymptomatic (A and B) and esca symptomatic (C and D) leaf midribs of grapevine plants are shown. After a first scan on intact leaves (A and C), the samples were cut (B and D) just above the scanned area to embolize the vessels and then scanned again. Air-filled (e.g. black arrowheads), water-filled (e.g. white arrowheads), and occluded (e.g. red arrowheads) vessels were counted and their cross-sectional diameters quantified to determine the PLC. The PLC represented by either native embolism (A and C) or occluded vessels (B and D) is given in parentheses. Bars = 100 μm.

The Nature of the Xylem Vessel Occlusions

We investigated the nature of the vessel occlusions causing the high percentage of nonfunctional vessels in esca symptomatic leaves using microCT and light microscopy. MicroCT was conducted both with and without the contrasting agent iohexol, which has been utilized previously to track the transpiration pathway and determine vessel functionality (as described by Pratt and Jacobsen [2018]). The subsequent robust (examining more than 200 cross sections per microCT volume) and detailed (examining both cross and longitudinal sections) examinations of the microCT volumes in symptomatic leaves revealed that the nature of the vessel occlusions is complex (Fig. 4). Occlusions can be larger, spanning the entire diameter of the vessel (Fig. 4A, red arrowheads), or smaller, occupying only a portion of the vessel (Fig. 4A, yellow arrowheads). Longitudinal sections of iohexol-fed symptomatic leaves revealed that the transpiration pathway can pass in between occlusions and through vessel connections (Fig. 4A, white arrowhead) but never diffuse in surrounding tissues. In asymptomatic samples fed with iohexol, occlusions expanding in iohexol-filled vessels were not observed (Supplemental Fig. S3). Some partially occluded vessels did not become air filled upon cutting (Fig. 4, B and C), and occlusions were also visible (although they were more obscure) in entirely occluded, nonfunctional vessels that did not fill with air after cutting (Fig. 4D, red arrowheads). When partially occluded vessels embolized after cutting, occlusions were easily visualized (Fig. 4E, red arrowheads). In these cases, the contact angle between these occlusions and the vessel wall was quantified and was always higher than 100°, with the highest frequency between 120° and 150° (Fig. 4F). Partially occluded vessels made up a small percentage of the total calculated PLC, representing 8.1% ± 3.7% for symptomatic midribs and 1.3% ± 0.6% for symptomatic petioles, while in asymptomatic leaves, partially occluded vessels were never observed (Supplemental Table S1). A negligible percentage of partially occluded vessels was observed within the native embolized vessels (i.e. air filled prior to cutting the samples), corresponding to 0.3% ± 0.2%

Table 1. *Effects of esca leaf symptom (asymptomatic or symptomatic), organ (midrib or petiole), and their interaction on the calculated PLC due to native embolism (Native PLC) and on the calculated PLC due to occlusions (Occlusion PLC)*

The plant was entered as a random effect in the models. Statistically significant results ($P < 0.05$) are shown in boldface. See the text for the model specificity for each trait.

Response Variable	Explanatory Variables	*F*	*P*
Native PLC (n = 35)	Leaf symptom	1.06	0.36
	Organ	0.37	0.61
	Interaction	2.53	0.25
Occlusion PLC (n = 35)	Leaf symptom	**14.32**	**0.02**
	Organ	1.99	0.29
	Interaction	0.61	0.52

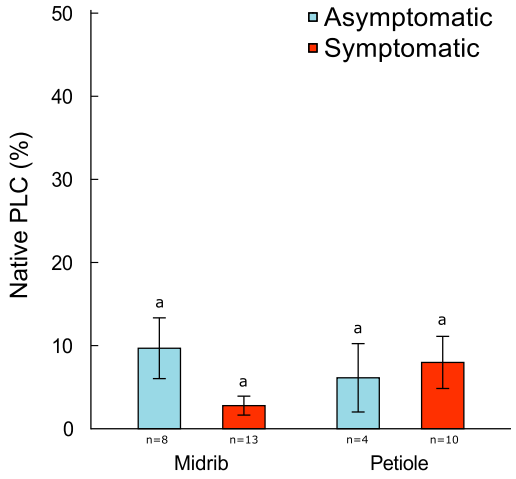

Figure 2. Mean native PLC in midribs and petioles of esca asymptomatic (blue) and esca symptomatic (red) leaves of grapevine plants using microCT imaging. PLC was calculated from the diameter of air-filled vessels in intact leaves, based on the total theoretical hydraulic conductivity of each sample. Error bars represent SE, and different letters represent statistically significant differences (least-squares mean differences of fixed effects, $P < 0.05$; n = sample size).

in symptomatic midribs and 0.4% ± 0.2% in symptomatic petioles (Supplemental Table S1).

The presence of these occlusions was likewise identified by light microscopy observations on symptomatic leaves (Fig. 5). To identify the chemical nature of the occlusions, cross sections were stained with four different dyes: Toluidine Blue O (Fig. 5A) in blue and periodic acid-Schiff reaction (Fig. 5B) in red indicate the presence of polysaccharides and polyphenols; Ruthenium Red (Fig. 5C) staining in pink for non-methyl-esterified pectins and Lacmoid Blue (Fig. 5D) showing the presence of callose in gray-pink shades. Quantifying the number of occluded vessels in histology cross sections of midribs, we found an average of 19.7% ± 11.6% of vessels with occlusions in symptomatic leaves, while just 0.4% ± 0.1% of vessels contained occlusions in asymptomatic leaves (Supplemental Table S2; Supplemental Fig. S4).

Relationship between Leaf Symptoms and Occlusion

Leaf symptom severity, quantified by the percentage of green tissue (in pixels) of each leaf, ranged from 6.1% to 93.9% for symptomatic leaves. In asymptomatic leaves, green tissue always accounted for 100%. We found no significant relationship between the percentage of green tissue (i.e. symptom severity) and PLC due to occluded vessels in symptomatic leaves ($F_{1,17} = 1.43$, $P = 0.25$; Fig. 6). Additionally, there was no significant relationship between the percentage of green tissue and PLC when analyzed by plant or by organ ($F_{3,17} = 0.31$, $P = 0.81$; $F_{1,17} = 0.80$, $P = 0.38$, respectively).

Fungi Detection

The two vascular pathogens, *P. chlamydospora* and *P. minimum*, were not detected in leaves or lignified shoots. In 2-year-old cordons, their presence was detected in some samples but not others, regardless of whether the vines were symptomatic or asymptomatic (Table 2). However, *P. chlamydospora* and *P. minimum* DNA was detected in 100% of trunks (from 23 vines) sampled in the same field plot. The average quantity of *P. chlamydospora* and *P. minimum* DNA in the trunks was 3.6 ± 0.7 and 3.7 ± 0.9 log fg ng^{-1} dry tissue, respectively.

DISCUSSION

To date, no study has investigated leaf xylem water transport and vessel integrity during vascular pathogenesis using real-time, noninvasive visualizations. Transplanting esca symptomatic vines (identified from years of survey) from the field to pots allowed the transport of the plants, enabling the use of synchrotron-based microCT to explore the relationship between vessel integrity and esca leaf symptom formation in intact vines at high resolution and in three dimensions. We demonstrate that gaseous embolism was not associated with esca leaf symptoms. Instead, most of the vessels in symptomatic leaves contained nongaseous embolisms formed by gels and/or tyloses, hindering water transport and possibly leading to hydraulic failure. Nevertheless, there was no positive correlation between the severity of esca leaf symptoms and the loss of theoretical hydraulic conductivity resulting from these vascular occlusions. The two common vascular

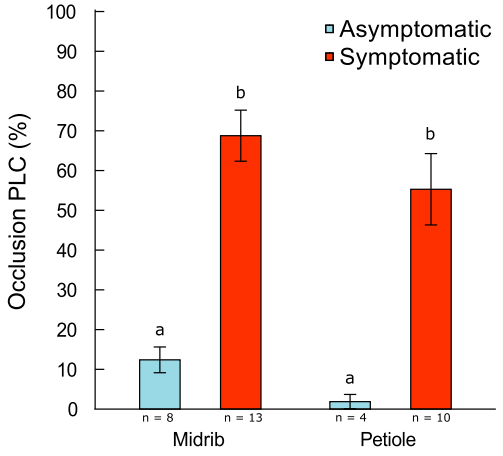

Figure 3. Mean occlusion PLC in midribs and petioles of esca asymptomatic (blue) and esca symptomatic (red) leaves of grapevine plants using microCT imaging. PLC was calculated from the diameter of occluded vessels, based on the total theoretical hydraulic conductivity of each sample. Error bars represent SE, and different letters represent statistically significant differences (least-squares mean differences of fixed effects, $P < 0.05$; n = sample size).

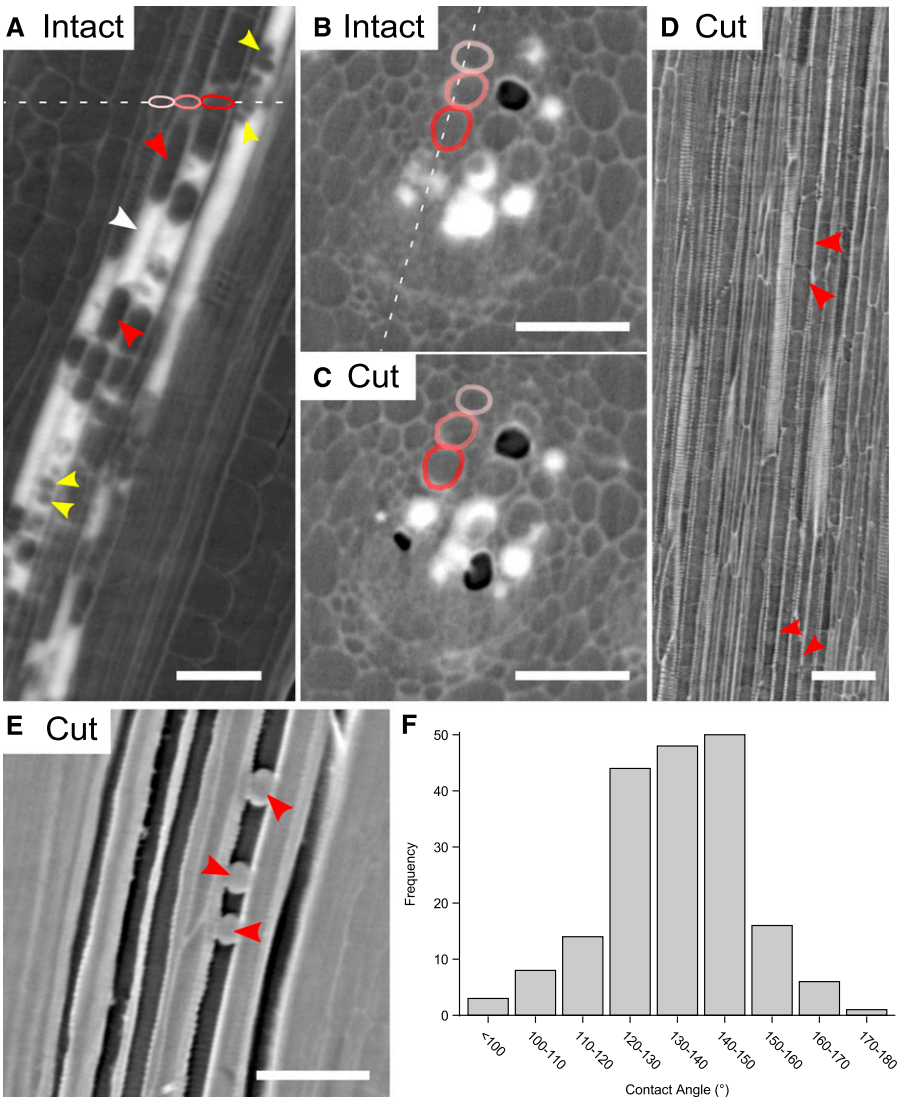

Figure 4. Two-dimensional reconstructions from microCT volumes of esca symptomatic leaves of grapevine. A to C, Iohexol-fed midrib viewed in a longitudinal section (A) and cross sections (B and C). For clarity and orientation, the same three vessels are color coded, and dotted lines represent the locations of the sections relative to each other. The contrasting agent iohexol appears bright white and allows for the identification of the water-transport pathway. The iohexol signal can even be seen in partially occluded vessels (e.g. white arrowhead). Occlusions (i.e. gels or tyloses) can span the entire diameter of the vessel (red arrowheads) or only a portion (yellow arrowheads). After a first scan on intact leaves (A and B), the sample was cut (C) just above the scanned area and scanned again. D, Longitudinal section of a midrib with completely occluded vessels. The presence of occlusions is visible (although obscure) inside the vessel lumen (red arrowheads). E, Longitudinal section of an air-filled midrib (after cutting) with clearly visible occlusions (red arrowheads). F, Frequency distribution of the contact angles between the occlusions and the vessel wall (sample size = 190). Bars = 100 μm.

pathogens related to esca were undetected in the vine's distal organs (i.e. annual stems and leaves), confirming that the symptoms and vascular occlusions occur at a distance from the pathogen niche localized in the trunk. Overall, these observations generate new perspectives regarding the nature and cause of esca leaf symptoms.

Native Embolism in Leaves

Vascular wilt diseases have been associated with significant levels of air embolism at the leaf level during oak (*Quercus* spp.) bacterial leaf scorch (McElrone et al., 2008) and at the stem level during pine (*Pinus* spp.) wilt and Pierce's disease (Umebayashi et al., 2011; Kuroda, 2012; Pérez-Donoso et al., 2016). In these cases, the formation of air embolism was speculated to result from the cell wall-degrading enzymatic activity of the pathogens (presumably to facilitate pathogen colonization through the vascular network). In our study, there were extremely low levels of native gaseous embolism in both esca symptomatic and asymptomatic leaves (petioles and midribs), demonstrating that symptom formation was not associated with the presence of air-filled vessels.

Leaf Xylem Occlusion: The Presence of Tyloses and Gels in Symptomatic Leaves

Under certain circumstances, xylem vessels can be occluded by tyloses (outgrowths from adjacent parenchyma cells through vessel pits; Zimmermann, 1979; De Micco et al., 2016) and/or gels (i.e. gums) composed of polysaccharides and pectins, which are secreted by parenchyma cells or directly by tyloses (Rioux et al., 1998). Tylose and/or gel formation is a general defense response of the plant against different biotic or abiotic stresses (Bonsen and Kučera, 1990; Beckman and Roberts, 1995; Sun et al., 2008). In this study, microCT imaging of leaf xylem vessels (both in petioles and midribs) revealed that all symptomatic leaves had

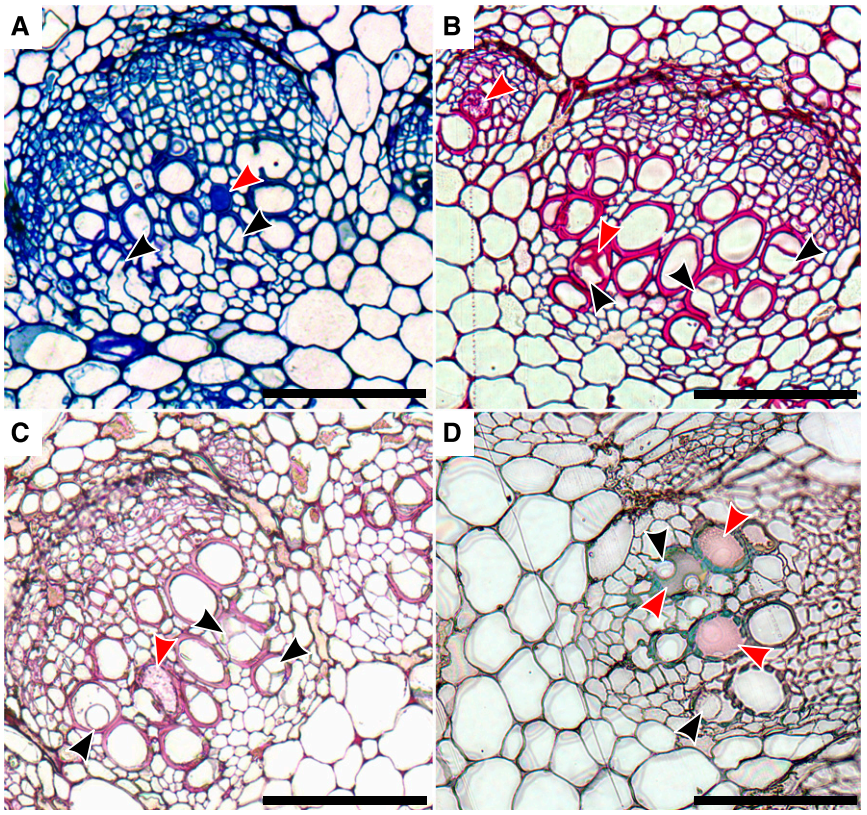

Figure 5. Light microscopy images of cross sections of esca symptomatic midribs of grapevine. Cross sections were stained with Toluidine Blue O (A), periodic acid-Schiff reaction (B), Ruthenium Red (C), and Lacmoid Blue (D). Red arrowheads indicate the presence of gels filling entirely the vessel lumen, while black arrowheads indicate the presence of tyloses in vessel lumina. Bars = 100 μm.

occluded vessels, although the loss of theoretical hydraulic conductance resulting from these occlusions was highly variable between leaves. Using reconstructions of 3D microCT volumes (Fig. 4) and light microscopy (Fig. 5), we determined that the occlusions in esca symptomatic leaves were due to both tyloses and gels. Numerous studies investigating vascular diseases have utilized artificial inoculation of the causal pathogen and observed the presence of vessel occlusions associated with decreases in hydraulic conductivity in either leaves or stems (Newbanks, 1983; Choat et al., 2009; Collins et al., 2009; Pouzoulet et al., 2017). The artificial inoculation in these studies resulted in high levels of the pathogen at the same location as the observed vascular occlusions. During esca pathogenesis in naturally infected vines, xylem occlusions were observed in 2-year-old symptomatic branches and in roots, and the pathogens were detected at the same locations (Gómez et al., 2016). In this study, the two vascular pathogen species associated with esca trunk necroses, *P. chlamydospora* and *P. minimum*, were not detected in current-year stems and leaves by a highly sensitive qPCR assay. This result was expected but had never been formally tested in the past according to the published literature. Thus, the vascular occlusions observed in leaves appeared to occur at some distance from the trunk, where the necroses are usually observed and both of the fungal species were detected (Bruez et al., 2014, 2016; Massonnet et al., 2018; Morales-Cruz et al., 2018), suggesting that vascular occlusions are caused by something other than the fungi themselves.

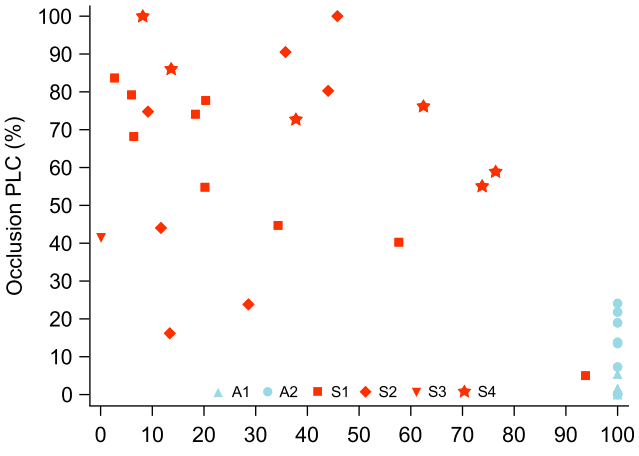

Figure 6. Relationship between the esca symptom severity (expressed as percentage of green tissue per leaf) and the theoretical loss of hydraulic conductivity due to occluded vessels (occlusion PLC) in midribs and petioles of grapevine. Points are grouped by plant: A1 and A2 (blue, asymptomatic) and S1 to S4 (red, symptomatic). The relationship between PLC and green tissue is not significant among symptomatic samples (red points, $P = 0.25$).

Light microscopy and histochemical analyses showed that occlusions are associated with the production of different compounds in symptomatic

Table 2. *Quantification by qPCR of* P. chlamydospora *and* P. minimum *(log fg ng^{-1} dry tissue)*

A high quantity of the DNA of the two pathogens was confirmed in 100% of the trunks of symptomatic plants sampled from the same vineyard (n = 23; see text for details). Values represent means ± SE in different organs; n = sample size. For esca leaf symptom, S = symptomatic and A = asymptomatic.

Pathogen	n	Esca	Petiole	First Internode	Fifth Internode	Multiyear Branches
P. chlamydospora	6	S	0	0	0	1.05 ± 0.58 (3/6)[a]
P. chlamydospora	6	A	0	0	0	1.13 ± 0.38 (4/6)[a]
P. minimum	6	S	0	0	0	1.48 ± 0.75 (3/6)[a]
P. minimum	6	A	0	0	0	0.59 ± 0.37 (2/6)[a]

[a]Number of samples positive for the pathogen.

leaves: polysaccharides, including pectins and callose. Grapevine is known to accumulate polyphenolic compounds during *P. chlamydospora* and *Phaeoacremonium* spp. infections (Del Rio et al., 2001; Martin et al., 2009) and in esca symptomatic leaves (Valtaud et al., 2009, 2011; Martín et al., 2019). Also, it is well documented that gels are composed of pectins (Rioux et al., 1998) and that parenchyma cells and tyloses accumulate pectin during vessel occlusion (Clérivet et al., 2000). In their review, Beckman and Roberts (1995) proposed a strong role of callose in tomato (*Solanum lycopersicum*) resistance to *Verticillium* spp., whereby callose xylem occlusions limit the spread of the pathogen. In this study, the presence of tyloses and gels (of any chemical nature) not colocalized with pathogens suggests that parenchyma cells play an important and active role during esca pathogenesis, expanding into the vessel lumen, secreting extracellular compounds, and eventually occluding the vessel.

Occlusions were clearly visible in partially occluded vessels that embolized after cutting, and the contact angle between the outside wall of occlusions and the inner vessel wall ranged mostly from 120° to 150° (Fig. 4, E and F). This result suggests that these occlusions are tyloses, as water droplets expanding into the vessels present lower contact angles (McCully et al., 2014).

Leaf Xylem Occlusion Occurs in Water-Filled Vessels

There are two main theories regarding the underlying mechanisms triggering vascular occlusion. Some studies have hypothesized the occlusions are always initiated by gaseous embolism and require the presence of air inside the vessel to stimulate the expansion of tyloses and/or the synthesis of gels (Zimmermann, 1978; Canny, 1997). Other studies suggest that gaseous embolism is not required and instead occlusion formation is stimulated by the plant hormone ethylene (Pérez-Donoso et al., 2007; Sun et al., 2007). Observations of samples fed with iohexol (Fig. 4A) demonstrated that occlusions were formed in water-filled vessels, suggesting that gaseous embolism is not necessary to induce occlusion formation in esca symptomatic leaves. In grapevine, similar occlusions in water-filled vessels were identified via microCT in grape berry pedicels associated with the onset of ripening (Knipfer et al., 2015).

The reconstruction of longitudinal sections of these vessels also demonstrated that the flow pathway can be extremely reticulate, moving between adjacent vessels and around occluded portions. Complex flow pathways such as these have been suggested previously by microCT-based flow modeling in grape (Lee et al., 2013), but this is the first direct empirical evidence supporting these models. In grape berry pedicels, partial occlusions are formed at the onset of ripening, yet despite a loss of conduit functionality, the pedicel hydraulic conductivity remained significantly high, suggesting a similar reticulate flow pathway in that context (Knipfer et al., 2015). The presence of partially occluded vessels that still conduct water around occluded portions confirms that occlusions were formed in functional water-filled vessels but creates difficulties with regard to interpreting images in cross section to determine vessel functionality. However, partially occluded vessels were found in very low percentage (1% in petioles and 8% in midribs; Supplemental Table S1), so they would not affect the loss of hydraulic conductivity estimated using microCT. In this study, we show examples of vessels that, when observed in a single cross section, appeared to be fully functional because of the clear iohexol signal (Fig. 4, B and C). However, when more comprehensive analyses of the volume are made (e.g. here with more than 200 cross sections per microCT volume), it became apparent that the iohexol signal was sometimes found in between occlusions (Fig. 4A). Therefore, quantifying occlusions from a limited number of cross sectional images could lead to an underestimation of the number of occluded vessels (Pérez-Donoso et al., 2016). This is well illustrated in our study, where the percentage of occluded vessels in midribs of symptomatic leaves was underestimated (only 19.7%) when examining a limited number of light microscopy images compared with microCT image analyses. Even more problematic for magnetic resonance imaging and microCT studies without the use of a mobile contrasting agent like iohexol, neither imaging technology appears capable of clearly distinguishing between functional, water-filled vessels and nonfunctional vessels filled by tyloses and/or gels. Only the use of robust volume analyses, in conjunction with contrasting agents, such as iohexol, can identify occlusions

in apparently water-filled vessels. The presence of visible occlusions after cutting the sample (Fig. 4E) complicates the interpretation regarding the effective functionality of the vessels. These partially occluded vessels represented only a maximum of 8% of the total conductivity (Supplemental Table S1) and should not significantly impact the overall PLC calculation. However, we can speculate that embolisms form even in these partially occluded vessels because (1) the vessel was still partially functional with space between the visible occlusion and the vessel wall (Fig. 4E) yet the resolution of the scan was not sufficient enough to visualize this space, (2) the water flow can avoid occlusions by passing through pits between vessels, or (3) grapevine leaves are able to secrete gels and tyloses in a very short period (i.e. during the few minutes between the cut and the end of the scan). Since we never observed occlusions remaining in air-filled vessels in asymptomatic samples, this third possibility also implies that symptomatic leaves are significantly more susceptible to occlusion than asymptomatic ones.

Leaf Symptoms, Occlusion, and Hypotheses on the Pathogenesis of Esca

Our results showed that there was no significant correlation between the level of leaf necrosis and the level of occluded vessels in symptomatic leaf midribs and petioles. Similarly, it has been shown that during Pierce's disease in grapevine, leaf symptoms are not correlated with the presence of the bacterial pathogen (Gambetta et al., 2007). Although many symptomatic leaves exhibited high levels of occlusion, many did not, and even leaves with high levels of scorched area can exhibit low levels of occlusion. The absence of any relationship between these variables could suggest that there is no causal relationship between xylem occlusions and esca leaf symptoms. However, it could have equally resulted because of the positions of our observations in relation to the way leaf necrosis proceeds. This study may have missed even more significant levels of vascular occlusion localized just at the front of the leaf necrosis (secondary order veins). In addition, we demonstrated that *P. chlamydospora* and *P. minimum* were not detected in the tissues of current-year petioles and stems but only in some of the 2-year-old branches sampled and always in the trunks of symptomatic plants. Altogether, these results demonstrate that symptom development was associated with vascular occlusions that are likely elicited at a distance from the pathogen niche localized in the trunk.

Hypotheses on the pathogenesis of esca largely fall into two broad categories: (1) the hydraulic failure hypothesis, where air embolism or vessel occlusion would disrupt the flow of sap in the xylem and lead to leaf desiccation; and (2) the elicitor-toxin hypothesis, where elicitors/toxins produced by the pathogenic fungi or plant-derived signals move into the vine's transpiration stream, inducing symptoms at a distance. The hydraulic failure hypothesis has never been properly tested, but observed decreases in stomatal conductance and photosynthesis in esca symptomatic leaves have been interpreted as supporting this hypothesis (Petit et al., 2006; Andreini et al., 2009; Magnin-Robert et al., 2011). Some studies call this into question because water stress-related genes are not overexpressed during esca symptom formation (Letousey et al., 2010; Fontaine et al., 2016). The elicitor/toxin hypothesis is supported by numerous works that aimed to identify phytotoxins and effectors secreted by fungal pathogens associated with esca and their potential contributions in disease etiology (Abou-Mansour et al., 2004; Bruno and Sparapano, 2006; Bruno et al., 2007; Luini et al., 2010; Masi et al., 2018). Other evidence is provided by the accumulation of antioxidant compounds prior to symptom expression in leaves (Valtaud et al., 2009; Magnin-Robert et al., 2011, 2016). Esca pathogenesis could also involve plant-derived signals (e.g. hormones, defense molecules, etc.) triggering and/or accelerating leaf senescence (Häffner et al., 2015). Although esca leaf symptoms often take a form that differs from natural senescence, the role of the senescence program in esca pathogenesis should be more thoroughly studied in the future. Natural leaf senescence includes many of the same changes (Salleo et al., 2002; Brodribb and Holbrook, 2003) that occur in esca symptomatic leaves: xylem vessel occlusion, decreases in stomatal conductance and photosynthesis, chlorosis, and eventually shedding. Some authors have also suggested a role for the senescence program in Pierce's disease pathogenesis (Choat et al., 2009).

The results presented here are consistent with the hypothesis that esca pathogens are restricted to the

Table 3. *Disease history of the grapevine 'Sauvignon blanc' plants used in this study*

Symptom frequency over time indicates the number of years with symptoms over the 6 or 5 years before transplantation.

Plant	Year of Transplantation	Symptom Frequency over Time (No. of Years)	Duration of Leaf Symptoms (Weeks) prior to the Moment of the Experiment
A1	2018	0/6	0
A2	2018	0/6	0
S1	2018	4/6	2
S2	2018	6/6	4
S3	2018	5/6	6
S4	2017	5/5	5

trunk and/or multiyear branches and that elicitors and/or toxins (for review, see Andolfi et al., 2011) become systematic in the plant via the transpiration stream, accumulate in the canopy, and trigger a cascade of events that lead to visual symptoms. These events include the production of tyloses and gels by the plant that occlude vessels, suggesting that the elicitor/toxin and hydraulic failure hypotheses are not necessarily mutually exclusive. This is also congruent with the observation of necrosis/oxidation along the vasculature that is spatially associated with leaf symptoms (Lecomte et al., 2012). The precise timing and direct impact of vessel occlusion relative to symptom formation remains unclear, so this study cannot determine whether occlusions lead to hydraulic failure and symptom formation or whether the observed vessel occlusion is simply a result of an early induced senescence process. Future research should be aimed at exploring this sequence of events leading to leaf scorch symptoms in naturally infected esca symptomatic vines in the field.

MATERIALS AND METHODS

Plant Material

Grapevine (*Vitis vinifera* 'Sauvignon blanc') plants aged 27 years old were transplanted from the field into pots from a vineyard at Institut National de la Recherche Agronomique (INRA) Aquitaine (44°47′24.8′′N, 0°34′35.1′′W). The transplantation was the only method allowing the study of natural esca symptom development on mature plants outside the field (greenhouse and synchrotron) and to bring the plants from Bordeaux (INRA) to Paris (synchrotron SOLEIL). The experimental plot included 343 plants organized in eight rows surveyed each season before transplantation for esca leaf symptom expression during the previous 5 to 6 years following Lecomte et al. (2012) leaf scorch symptom description. Esca incidence in this vineyard was very high, as 77% of the plants (n = 343 plants) presented trunk and/or leaf symptoms the summer before the plants were uprooted. The presence of two vascular fungi associated with esca (*Phaeomoniella chlamydospora* and *Phaeoacremonium minimum*) in this plot was confirmed by using qPCR on the trunk of 23 symptomatic vines randomly sampled (methodology described below). To reduce stressful events, the plants were excavated during dormancy before bud burst in late winter from the field by digging around the woody root system and attempting to preserve as many of the large woody roots as possible. Following excavation, the root system was immersed under water overnight, and then powdered with indole-3-butyric acid to promote rooting. To equilibrate the vigor of the plants and their leaf-root ratio, three to five buds per arm (one per side) were left. The plants were potted in 20-L pots in fine clay medium (Klasmann Deilmann substrate 4:264) and placed indoors for 2 months on heating plates (30°C) to encourage root development before they were transferred to a greenhouse and irrigated to capacity every other day under natural light. Plants were irrigated with nutritive solution (0.1 mM $NH_4H_2PO_4$, 0.187 mM NH_4NO_3, 0.255 mM KNO_3, 0.025 mM $MgSO_4$, 0.002 mM Fe, and oligo-elements [B, Zn, Mn, Cu, and Mo]) to prevent mineral deficiencies.

Plants were grown in a greenhouse and exposed to natural light. Temperature and air relative humidity were monitored every 30 min: average daily values corresponded to 26°C ± 4°C (SE) and 64% ± 13% (SE), respectively. Leaf predawn water potential was monitored regularly to ensure that the plants were never water stressed (leaf predawn water potential close to 0 MPa). The plants were surveyed weekly for esca leaf symptom development from May to September. The plants were noted as symptomatic when at least 50% of the canopy was presenting the tiger-stripe leaf symptom, characteristic for esca (see examples of leaf symptoms in Supplemental Fig. S5A and entire plants in Supplemental Fig. S5B). Six plants were selected (Table 3) and transferred to the microCT PSICHE (Pressure Structure Imaging by Contrast at High Energy) beamline (SOLEIL synchrotron facility, Saclay, France): two control asymptomatic plants that had never expressed symptoms either during the year of the experiment or the past 5 years, and four symptomatic plants with differences in the timing of the first leaf symptom expression (6, 5, 4, and 2 weeks before the experiment). Leaf symptoms (Supplemental Fig. S5) were typical esca leaf symptoms for cv Sauvignon blanc and were similar to the symptoms we observed in the experimental vineyard from which the plants came. All symptomatic plants had expressed esca symptoms for at least three different seasons in the past (Table 3). Asymptomatic leaves were always sampled only from the control plants A1 and A2.

MicroCT

Synchrotron-based microCT was used to visualize the contents of vessels in the esca symptomatic and asymptomatic leaf midribs and petioles. The PSICHE beamline at the SOLEIL synchrotron facility that is dedicated to x-ray diffraction under extreme conditions (pressure-temperature) and to high energy absorption contrast tomography (20–50 keV) was used (King et al., 2016). During the first campaign, in September 2017, one 26-year-old plant presenting characteristic tiger-stripe leaf symptoms was scanned with the microCT PSICHE beamline (King et al., 2016). In the second campaign, in September 2018, five different plants of the same age (two asymptomatic and three symptomatic) were brought to the same facility. Intact shoots (>1.5 m in length) were cut at the base under water at least 1 m away from the scanned leaves. Leaves were scanned using a high-flux (3×10^{11} photons mm^{-2}) 25-keV monochromatic x-ray beam. Midribs (n = 21) and petioles (n = 15) were scanned in symptomatic and asymptomatic leaves (from one to five leaves per plant), then cut just above the scanned area and scanned again. The projections were recorded with a Hamamatsu Orca Flash sCMOS camera equipped with a 250-μm-thick LuAG scintillator for petioles and with a 90-μm-thick LuAG scintillator for midribs. The complete tomographic scan included 1500 projections, and each projection lasted 50 ms for petioles and 200 ms for midribs. Thus, the total exposure time was 75 s for petioles and 300 s for midribs. Tomographic reconstructions were performed using PyHST2 software (Mirone et al., 2014) using the Paganin method (Paganin et al., 2002), resulting in 32-bit volume reconstructions of $2,048 \times 2,048 \times 1,024$ voxels for petioles and $2,048 \times 2,048 \times 2,048$ voxels for midribs. The final spatial resolution was 2.8769^3 μm^3 per voxel for petioles and 0.8601^3 μm^3 for midribs.

Iohexol Contrasting Agent

A subset of 10 shoots were fed with the contrasting agent iohexol. Five symptomatic shoots (from two plants: S1 and S2 described in Table 3) and five asymptomatic shoots (from two plants: A1 and A2 described in Table 3) were cut at the base under water and immediately transferred to a solution containing the contrasting agent iohexol (150 mM) to visualize functionality (i.e. vessels that were effectively transporting sap; Pratt and Jacobsen, 2018). In asymptomatic plants, five midribs (from three different shoots) and three petioles (from two different shoots), and in symptomatic plants, five midribs (from three different shoots) and four petioles (from three different shoots), were scanned. These shoots were exposed to sunlight outdoors for at least half a day to permit the contrasting agent to reach the leaves through transpiration. The capacity and rapidity of iohexol to move was first checked by cutting leaves under water, submerging them directly in iohexol solution, and scanning several times each 10 min. Its capacity to move up to the shoots was then checked by scanning leaves at the top. These results were not coupled with the ones from intact leaf scans. In this case, scans were performed at two different energies, just below and just above the iodine K-edge of 33.2 keV. At 33.1 keV, the contrasting agent presents little contrast, while it presents strong contrast at 33.3 keV. The leaves (17 of 35 total samples) were then analyzed in the beamline as described for the other samples above.

Image Analysis

Leaf Symptoms

Scanned leaves were photographed, and the green area was calculated using the G. Landini plug-in threshold_color v1.15 (http://www.mecourse.com/landinig/software/software.html) in ImageJ software (http://rsb.info.nih.gov/ij), differentiating four color regions: red, yellow, pale green, and green. The number of pixels for each region was summed to determine the leaf area corresponding to each color region. To obtain a scale of symptom severity, the percentage of green leaf area (relative to total leaf area) was calculated for each leaf.

Analysis of MicroCT Images

All samples (including those stained with iohexol) were analyzed in the following manner. The geometrical diameter of air-filled and non-air-filled vessels was measured on cross sections taken from the central slice of the microCT scanned volume using ImageJ software. For iohexol-fed samples, an example of vessel identification is included in Supplemental Figure S6. The theoretical hydraulic conductivity of each vessel was calculated using the Hagen-Poiseuille equation:

$$\mathrm{Kh} = \frac{(\pi \times {}^{4} \times \rho)}{(128 \times \eta)} \quad (1)$$

where *Kh* is the theoretical hydraulic conductivity ($m^4\ MPa^{-1}\ s^{-1}$), ø is the geometrical diameter of the vessel (m), ρ is the density of water ($kg\ m^{-3}$), and η the viscosity of water (1.002 mPa s^{-1} at 20°C). The percentage of native embolism was calculated in the first scan, before cutting the leaf, using the following equation:

$$\text{Native PLC } (\%) = 100 \times \frac{(\Sigma\ \mathrm{Kh}_{\text{air filled vessels}})}{(\Sigma\ \mathrm{Kh}_{\text{all vessels}})} \quad (2)$$

After a first scan, the samples were cut with a clean razor blade just above the scanned area and scanned again. Cut open vessels will embolize because the xylem sap is under negative pressure. Leaf water potential (Ψ_L) measured on an adjacent leaf just after the scan indicated sufficient tension in the xylem sap to embolize in all leaves measured ($n = 17$ leaves, $\Psi_L = -0.46$ MPa on average). Under control conditions, nearly all the xylem vessels became air filled upon cutting (e.g. black vessels in Fig. 1B; Supplemental Fig. S1B). To estimate the loss of conductivity caused by occluded vessels (Eq. 3 below), the *Kh* of apparent water-filled vessels was calculated in the central cross section of the entire microCT volume after cutting. Vessels that did not become completely air filled after cutting were considered occluded (i.e. having the same gray level after cutting as water-filled conduits before cutting). To adjust PLC (Eq. 3 presented below) by those vessels that appeared water filled or air filled only at specific points along the length of the vessel, the presence of apparent water-filled vessels and droplets was checked in at least 200 cross sectional slices in each volume, corresponding to 160 μm for midribs and 570 μm for petioles. If a particular vessel appeared water filled in any of the 200 slices examined, this vessel was classified as partially occluded and added to the PLC given by occlusions:

$$\text{Occlusion PLC } (\%) = 100 \times \frac{(\Sigma\ \mathrm{Kh}_{\text{occluded vessels}} + \Sigma\ \mathrm{Kh}_{\text{partially occluded vessels}})}{(\Sigma\ \mathrm{Kh}_{\text{all vessels}})} \quad (3)$$

Contact Angles

To gain insight into the nature of occlusion, the contact angle between each droplet and the inner vessel wall was measured using ImageJ following McCully et al. (2014). First longitudinal slices were reconstructed from each microCT volume. Then the contact angles between each observed droplet and the vessel wall were measured in partially occluded, air-filled vessels ($n = 190$ droplets from 65 partially occluded vessels in two different samples).

Light Microscopy

Ten-millimeter sections from midribs and petioles of three esca symptomatic and three asymptomatic leaves were cut and fixed in a solution containing 0.64% (v/v) paraformaldehyde, 50% (v/v) ethanol, 5% (v/v) acetic acid, and 44.36% (v/v) water. Samples were then dehydrated using a graded series of ethanol (50%, 70%, 85%, 95%, 100%, 100%, and 100% [v/v] for 30 min each) and embedded using a graded series of LR White resin (Agar Scientific; 33%, 50%, and 66% [v/v] LR White in ethanol solutions for 120 min each and 100% [v/v] LR White three times overnight). Two- to 2.5-μm-thick transverse sections were cut using an Ultracut S microtome (Reichert) equipped with a glass knife. As described by Neghliz et al. (2016), the cross section was stained with different dyes. To investigate anatomical features, lignin, phenolic compound, and polysaccharide cross sections were stained with 0.05% (w/v) Toluidine Blue O. Sections to be examined for polysaccharides were stained with periodic acid-Schiff reagent. Pectins were detected by staining sections overnight with 1% (w/v) Ruthenium Red. Callose was revealed by staining sections overnight with 1% (w/v) Lacmoid Blue in 3% (v/v) acetic acid. Stained sections were dried and photographed with a RTKE camera (Spot) mounted on an Axiophot microscope (Zeiss) at the Bordeaux Imaging Center, a member of the France Bio Imaging national infrastructure (ANR-10-INBS-04). In midribs, the image of the entire cross section was analyzed to quantify the percentage of occluded vessels (by tyloses, gels, or both) in 55 sections for symptomatic and 56 sections for asymptomatic midribs obtained from six different leaves (three symptomatic and three asymptomatic). Occlusions were classified as tyloses if tylose cell walls (formed during tylosis development) were visualized within the vessel lumen (Fig. 5B) or as gels if cell walls were not visualized and the vessel lumen appeared totally filled (Fig. 5A, red arrowheads). Tyloses and gels can also be observed within the same vessel (Fig. 5D). In some cases, tyloses and gels can be difficult to distinguish if tyloses filled the entire vessel lumen with a wall closely attached to the inner vessel wall, or if the tylose wall was lignified. However, this uncertainty would not change the total number of occluded vessels observed in this study.

Fungal Detection

The presence of *P. chlamydospora* and *P. minimum* was assessed in different parts of asymptomatic and symptomatic plants. Plants were sampled directly from the same field plot as described above. In mid-August 2018, a survey of leaf esca symptoms was conducted, and six asymptomatic and six symptomatic vines were selected at random. Four different samples were collected for each plant: (1) petioles of three leaves located in the first 50 cm of the shoot; sections of the (2) first and (3) fifth internodes of the third shoot on the 2-year-old cane; and (4) a section of the 2-year-old branch just basal to the third shoot (i.e. canes trained across in the Guyot system). These organs were focused on as they are typically not used to detect esca pathogens, which have mainly been observed in the trunk. However, to control the presence of these fungi in the trunk, 23 symptomatic plants were randomly sampled from the same plot by drilling 1 cm at the same height in each trunk. All samples were collected using ethyl alcohol-sterilized pruning shears and placed immediately in liquid nitrogen. DNA extraction and qPCR analysis were conducted as previously described by Pouzoulet et al. (2013, 2017) using the primer sets PchQF/R and PalQF/R. Briefly, samples were lyophilized for 48 h. After the bark and pith were removed from the samples (except for petioles) using a sterile scalpel, samples were ground and DNA was extracted as described by Pouzoulet et al. (2013). Quantification of *P. chlamydospora* and *P. minimum* DNA by qPCR (SYBR Green assays) was conducted as described by Pouzoulet et al. (2017). Pathogen DNA quantity was normalized by the amount of total DNA used as template, and the mean of three technical replicates was used for further analysis.

Statistical Analysis

The effects of leaf symptom (asymptomatic or symptomatic), organ (midrib or petiole), and their interaction on the calculated native PLC and on the PLC due to occluded vessels were tested using PROC GLIMMIX in SAS software (SAS 9.4; SAS Institute). The plant was entered into models as a random effect, since different leaves were sometimes scanned from the same plant (from one to five per plant). Proportional data (ranging from 0 to 1, dividing all PLC data by 100) was analyzed to fit a logit link function and binomial distribution as appropriate. We computed pairwise least-squares mean differences of fixed effects. The effect of symptom severity (expressed as the percentage of green tissue) among symptomatic leaves on PLC was tested as described above including the plant and organ as covariables (fixed effects) in the model.

Supplemental Data

The following supplemental materials are available.

Supplemental Figure S1. Two-dimensional reconstructions of cross sections from microCT volumes and optical microscopy cross sections of grapevine leaf petioles.

Supplemental Figure S2. Two-dimensional reconstructions of longitudinal and cross sections from microCT volumes of grapevine leaf midribs.

Supplemental Figure S3. Two-dimensional reconstructions of longitudinal and cross sections from microCT volumes for esca asymptomatic leaf midribs scanned on iohexol-fed grapevine shoots.

Supplemental Figure S4. Light microscopy images of cross sections of esca asymptomatic midribs of grapevine.

Supplemental Figure S5. Images of asymptomatic control and esca symptomatic plants of grapevine cv Sauvignon blanc.

Supplemental Figure S6. Method used for vessel segmentation in iohexol-fed grapevine petioles.

Supplemental Table S1. Calculated theoretical conductivity from microCT volumes.

Supplemental Table S2. Quantification of not-filled and occluded vessels in a histological photomicrograph of grapevine midribs.

ACKNOWLEDGMENTS

We thank the experimental teams of UMR SAVE and UMR EGFV (Bord'O platform, INRA, Bordeaux, France) and the SOLEIL synchrotron facility (HRCT beamline PSICHE) for providing the materials and logistics. We thank Jérôme Jolivet (UMR SAVE) for providing technical knowledge and support for plant transplantation and Brigitte Batailler (Bordeaux Imaging Center) for providing technical support for the light microscopy sample preparation.

Received June 24, 2019; accepted August 9, 2019; published August 27, 2019.

LITERATURE CITED

Abou-Mansour E, Couché E, Tabacchi R (2004) Do fungal naphthalenones have a role in the development of esca symptoms? Phytopathol Mediterr **43:** 75–82

Andolfi A, Mugnai L, Luque J, Surico G, Cimmino A, Evidente A (2011) Phytotoxins produced by fungi associated with grapevine trunk diseases. Toxins (Basel) **3:** 1569–1605

Andreini L, Caruso G, Bertolla C, Scalabrelli G, Viti R, Gucci R (2009) Gas exchange, stem water potential and xylem flux on some grapevine cultivars affected by esca disease. S Afr J Enol Vitic **30:** 2

Beckman CH, Roberts EM (1995) On the nature and genetic basis for resistance and tolerance to fungal wilt diseases of plants. In Adv Bot Res, Vol **21**. pp 35–77

Bertsch C, Ramírez-Suero M, Magnin-Robert M, Larignon P, Chong J, Abou-Mansour E, Spagnolo A, Clément C, Fontaine F (2013) Grapevine trunk diseases: Complex and still poorly understood. Plant Pathol **62:** 243–265

Bonsen KJM, Kučera LJ (1990) Vessel occlusions in plants: Morphological, functional and evolutionary aspects. IAWA J **11:** 393–399

Brodribb TJ, Holbrook NM (2003) Stomatal closure during leaf dehydration, correlation with other leaf physiological traits. Plant Physiol **132:** 2166–2173

Bruez E, Baumgartner K, Bastien S, Travadon R, Guérin-Dubrana L, Rey P (2016) Various fungal communities colonise the functional wood tissues of old grapevines externally free from grapevine trunk disease symptoms. Aust J Grape Wine Res **22:** 288–295

Bruez E, Vallance J, Gerbore J, Lecomte P, Da Costa JP, Guerin-Dubrana L, Rey P (2014) Analyses of the temporal dynamics of fungal communities colonizing the healthy wood tissues of esca leaf-symptomatic and asymptomatic vines. PLoS ONE **9:** e95928

Bruno G, Sparapano L (2006) Effects of three esca-associated fungi on *Vitis vinifera* L. III. Enzymes produced by the pathogens and their role in fungus-to-plant or in fungus-to-fungus interactions. Physiol Mol Plant Pathol **69:** 182–194

Bruno G, Sparapano L, Graniti A (2007) Effects of three esca-associated fungi on *Vitis vinifera* L. IV. diffusion through the xylem of metabolites produced by two tracheiphilous fungi in the woody tissue of grapevine leads to esca-like symptoms on leaves and berries. Physiol Mol Plant Pathol **71:** 106–124

Canny M (1997) Tyloses and the maintenance of transpiration. Ann Bot (Lond) **80:** 565–570

Choat B, Gambetta GA, Wada H, Shackel KA, Matthews MA (2009) The effects of Pierce's disease on leaf and petiole hydraulic conductance in *Vitis vinifera* cv. Chardonnay. Physiol Plant **136:** 384–394

Clérivet A, Déon V, Alami I, Lopez F, Geiger JP, Nicole M (2000) Tyloses and gels associated with cellulose accumulation in vessels are responses of plane tree seedlings (*Platanus* × *acerifolia*) to the vascular fungus *Ceratocystis fimbriata* f. sp *platani*. Trees (Berl) **15:** 25–31

Cloete M, Mostert L, Fischer M, Halleen F (2015) Pathogenicity of South African Hymenochaetales taxa isolated from esca-infected grapevines. Phytopathol Mediterr **54:** 368–379

Collins BR, Parke JL, Lachenbruch B, Hansen EM (2009) The effects of *Phytophthora ramorum* infection on hydraulic conductivity and tylosis formation in tanoak sapwood. Can J For Res **39:** 1766–1776

Del Rio JA, Gonzalez A, Fuster MD, Botia JM, Gomez P, Frias V, Ortuno A (2001) Tylose formation and changes in phenolic compounds of grape roots infected with *Phaeomoniella chlamydospora* and *Phaeoacremonium* species. Phytopathol Mediterr **40:** S394–S399

De Micco V, Balzano A, Wheeler EA, Baas P (2016) Tyloses and gums: A review of structure, function and occurrence of vessel occlusions. IAWA J **37:** 186–205

Feliciano AJ, Eskalen A, Gubler WD (2004) Differential susceptibility of three grapevine cultivars to the *Phaeoacremoium aleophilum* and *Phaeomoniella chlamydospora* in California. Phytopathol Mediterr **43:** 66–69

Fischer M (2006) Biodiversity and geographic distribution of basidiomycetes causing esca-associated white rot in grapevine: A worldwide perspective. Phytopathol Mediterr **45:** S30–S42

Fischer M, Peighami-Ashnaei S (2019) Grapevine, esca complex, and environment: The disease triangle. Phytopathol Mediterr **58:** 17–37

Fisher PJ, Petrini O, Sutton BC (1993) A comparative study of fungal endophytes in leaves, xylem and bark of Eucalyptus in Australia and England. Sydowia **45:** 338–345

Fontaine F, Pinto C, Vallet J, Clément C, Gomes AC, Spagnolo A (2016) The effects of grapevine trunk diseases (GTDs) on vine physiology. Eur J Plant Pathol **144:** 707–721

Fradin EF, Thomma BP (2006) Physiology and molecular aspects of *Verticillium* wilt diseases caused by *V. dahliae* and *V. albo-atrum*. Mol Plant Pathol **7:** 71–86

Gambetta GA, Fei J, Rost TL, Matthews MA (2007) Leaf scorch symptoms are not correlated with bacterial populations during Pierce's disease. J Exp Bot **58:** 4037–4046

Gómez P, Báidez AG, Ortuño A, Del Río JA (2016) Grapevine xylem response to fungi involved in trunk diseases: Grapevine vascular defence. Ann Appl Biol **169:** 116–124

Gramaje D, Úrbez-Torres JR, Sosnowski MR (2018) Managing grapevine trunk diseases with respect to etiology and epidemiology: Current strategies and future prospects. Plant Dis **102:** 12–39

Guerin-Dubrana L, Fontaine F, Mugnai L (2019) Grapevine trunk disease in European and Mediterranean vineyards: Occurrence, distribution and associated disease-affecting cultural factors. Phytopathol Mediterr **58:** 49–71

Häffner E, Konietzki S, Diederichsen E (2015) Keeping control: The role of senescence and development in plant pathogenesis and defense. Plants (Basel) **4:** 449–488

King A, Guignot N, Zerbino P, Boulard E, Desjardins K, Bordessoule M, Leclerq N, Le S, Renaud G, Cerato M, et al (2016) Tomography and imaging at the PSICHE beam line of the SOLEIL synchrotron. Rev Sci Instrum **87:** 93704

Knipfer T, Fei J, Gambetta GA, McElrone AJ, Shackel KA, Matthews MA (2015) Water transport properties of the grape pedicel during fruit development: Insights into xylem anatomy and function using microtomography. Plant Physiol **168:** 1590–1602

Kuroda K (2012) Monitoring of xylem embolism and dysfunction by the acoustic emission technique in *Pinus thunbergii* inoculated with the pine wood nematode *Bursaphelenchus xylophilus*. J For Res **17:** 58–64

Larignon P, Dubos B (1997) Fungi associated with esca disease in grapevine. Eur J Plant Pathol **10:** 147–157

Lecomte P, Darrieutort G, Liminana JM, Comont G, Muruamendiaraz A, Legorburu FJ, Choueiri E, Jreijiri F, El Amil R, Fermaud M (2012) New insights into esca of grapevine: The development of foliar symptoms and their association with xylem discoloration. Plant Dis **96:** 924–934

Lee EF, Matthews MA, McElrone AJ, Phillips RJ, Shackel KA, Brodersen CR (2013) Analysis of HRCT-derived xylem network reveals reverse flow in some vessels. J Theor Biol **333:** 146–155

Letousey P, Baillieul F, Perrot G, Rabenoelina F, Boulay M, Vaillant-Gaveau N, Clément C, Fontaine F (2010) Early events prior to visual symptoms in the apoplectic form of grapevine esca disease. Phytopathology **100:** 424–431

Luini E, Fleurat-Lessard P, Rousseau L, Roblin G, Berjeaud JM (2010) Inhibitory effects of polypeptides secreted by the grapevine pathogens Phaeomoniella chlamydospora and Phaeoacremonium aleophilum on plant cell activities. Physiol Mol Plant Pathol **74:** 403–411

Magnin-Robert M, Letousey P, Spagnolo A, Rabenoelina F, Jacquens L, Mercier L, Clément C, Fontaine F (2011) Leaf stripe form of esca induces alteration of photosynthesis and defence reactions in presymptomatic leaves. Funct Plant Biol **38:** 856–866

Magnin-Robert M, Spagnolo A, Boulanger A, Joyeux C, Clément C, Abou-Mansour E, Fontaine F (2016) Changes in plant metabolism and accumulation of fungal metabolites in response to esca proper and apoplexy expression in the whole grapevine. Phytopathology **106:** 541–553

Martín L, Fontaine F, Castaño FJ, Songy A, Roda R, Vallet J, Ferrer-Gallego R (2019) Specific profile of Tempranillo grapevines related to Esca-leaf symptoms and climate conditions. Plant Physiol Biochem **135:** 575–587

Martin N, Vesentini D, Rego C, Monteiro S, Oliveira H, Ferreira RB (2009) *Phaeomoniella chlamydospora* infection induces changes in phenolic compounds content in *Vitis vinifera*. Phytopathol Mediterr **48:** 101–116

Masi M, Cimmino A, Reveglia P, Mugnai L, Surico G, Evidente A (2018) Advances on fungal phytotoxins and their role in grapevine trunk diseases. J Agric Food Chem **66:** 5948–5958

Massonnet M, Morales-Cruz A, Minio A, Figueroa-Balderas R, Lawrence DP, Travadon R, Rolshausen PE, Baumgartner K, Cantu D (2018) Whole-genome resequencing and pan-transcriptome reconstruction highlight the impact of genomic structural variation on secondary metabolite gene clusters in the grapevine esca pathogen *Phaeoacremonium minimum*. Front Microbiol **9:** 1784

McCully M, Canny M, Baker A, Miller C (2014) Some properties of the walls of metaxylem vessels of maize roots, including tests of the wettability of their lumenal wall surfaces. Ann Bot **113:** 977–989

McElrone AJ, Grant JA, Kluepfel DA (2010) The role of tyloses in crown hydraulic failure of mature walnut trees afflicted by apoplexy disorder. Tree Physiol **30:** 761–772

McElrone AJ, Jackson S, Habdas P (2008) Hydraulic disruption and passive migration by a bacterial pathogen in oak tree xylem. J Exp Bot **59:** 2649–2657

Mirone A, Gouillart E, Brun E, Tafforeau P, Kieffer J (2014) PyHST2: An hybrid distributed code for high speed tomographic reconstruction with iterative reconstruction and a priori knowledge capabilities. Nucl Instrum Methods Phys Res B **324:** 41–48

Mondello V, Larignon P, Armengol J, Kortekamp A, Vaczy K, Prezman F, Serrano E, Rego C, Mugnai L, Fontaine F (2018) Management of grapevine trunk diseases: Knowledge transfer, current strategies and innovative strategies adopted in Europe. Phytopathol Mediterr **57:** 369–383

Morales-Cruz A, Allenbeck G, Figueroa-Balderas R, Ashworth VE, Lawrence DP, Travadon R, Smith RJ, Baumgartner K, Rolshausen PE, Cantu D (2018) Closed-reference metatranscriptomics enables in planta profiling of putative virulence activities in the grapevine trunk disease complex. Mol Plant Pathol **19:** 490–503

Mugnai L, Graniti A, Surico G (1999) Esca (black measles) and brown wood-streaking: Two old and elusive diseases of grapevines. Plant Dis **83:** 404–418

Neghliz H, Cochard H, Brunel N, Martre P (2016) Ear rachis xylem occlusion and associated loss in hydraulic conductance coincide with the end of grain filling for wheat. Front Plant Sci **7:** 920

Newbanks D (1983) Evidence for xylem dysfunction by embolization in Dutch elm disease. Phytopathology **73:** 1060

Oliva J, Stenlid J, Martínez-Vilalta J (2014) The effect of fungal pathogens on the water and carbon economy of trees: Implications for drought-induced mortality. New Phytol **203:** 1028–1035

Oses R, Valenzuela S, Freer J, Sanfuentes E, Rodriguez J (2008) Fungal endophytes in xylem of healthy Chilean trees and their possible role in early wood decay. Fungal Divers **33:** 77–86

Paganin D, Mayo SC, Gureyev TE, Miller PR, Wilkins SW (2002) Simultaneous phase and amplitude extraction from a single defocused image of a homogeneous object. J Microsc **206:** 33–40

Pearce RB (1996) Antimicrobial defences in the wood of living trees. New Phytol **132:** 203–233

Pérez-Donoso AG, Greve LC, Walton JH, Shackel KA, Labavitch JM (2007) *Xylella fastidiosa* infection and ethylene exposure result in xylem and water movement disruption in grapevine shoots. Plant Physiol **143:** 1024–1036

Pérez-Donoso AG, Lenhof JJ, Pinney K, Labavitch JM (2016) Vessel embolism and tyloses in early stages of Pierce's disease. Aust J Grape Wine Res **22:** 81–86

Petit AN, Vaillant N, Boulay M, Clément C, Fontaine F (2006) Alteration of photosynthesis in grapevines affected by esca. Phytopathology **96:** 1060–1066

Pouzoulet J, Mailhac N, Couderc C, Besson X, Daydé J, Lummerzheim M, Jacques A (2013) A method to detect and quantify *Phaeomoniella chlamydospora* and *Phaeoacremonium aleophilum* DNA in grapevine-wood samples. Appl Microbiol Biotechnol **97:** 10163–10175

Pouzoulet J, Pivovaroff AL, Santiago LS, Rolshausen PE (2014) Can vessel dimension explain tolerance toward fungal vascular wilt diseases in woody plants? Lessons from Dutch elm disease and esca disease in grapevine. Front Plant Sci **5:** 253

Pouzoulet J, Scudiero E, Schiavon M, Rolshausen PE (2017) Xylem vessel diameter affects the compartmentalization of the vascular pathogen *Phaeomoniella chlamydospora* in grapevine. Front Plant Sci **8:** 1442

Pratt RB, Jacobsen AL (2018) Identifying which conduits are moving water in woody plants: A new HRCT-based method. Tree Physiol **38:** 1200–1212

Qi F, Jing T, Zhan Y (2012) Characterization of endophytic fungi from *Acer ginnala* Maxim. in an artificial plantation: Media effect and tissue-dependent variation. PLoS ONE **7:** e46785

Reis P, Pierron R, Larignon P, Lecomte P, Abou-Mansour E, Farine S, Bertsch C, Jacques A, Trotel-Aziz P, Rego C, et al (2019) *Vitis* methods to understand and develop strategies for diagnosis and sustainable control of grapevine trunk diseases. Phytopathology **109:** 916–931

Rioux D, Nicole M, Simard M, Ouellette GB (1998) Immunocytochemical evidence that secretion of pectin occurs during gel (gum) and tylosis formation in trees. Phytopathology **88:** 494–505

Salleo S, Nardini A, Lo Gullo MA, Ghirardelli LA (2002) Changes in stem and leaf hydraulics preceding leaf shedding in *Castanea sativa* L. Biol Plant **45:** 227–234

Sun Q, Rost TL, Matthews MA (2008) Wound-induced vascular occlusions in Vitis vinifera (Vitaceae): Tyloses in summer and gels in winter. Am J Bot **95:** 1498–1505

Sun Q, Rost TL, Reid MS, Matthews MA (2007) Ethylene and not embolism is required for wound-induced tylose development in stems of grapevines. Plant Physiol **145:** 1629–1636

Sun Q, Sun Y, Walker MA, Labavitch JM (2013) Vascular occlusions in grapevines with Pierce's disease make disease symptom development worse. Plant Physiol **161:** 1529–1541

Surico G, Mugnai L, Marchi G (2006) Older and more recent observations on esca: A critical overview. Phytopathol Mediterr **45:** S68–S86

Torres-Ruiz JM, Jansen S, Choat B, McElrone AJ, Cochard H, Brodribb TJ, Badel E, Burlett R, Bouche PS, Brodersen CR, et al (2015) Direct x-ray microtomography observation confirms the induction of embolism upon xylem cutting under tension. Plant Physiol **167:** 40–43

Umebayashi T, Fukuda K, Haishi T, Sotooka R, Zuhair S, Otsuki K (2011) The developmental process of xylem embolisms in pine wilt disease monitored by multipoint imaging using compact magnetic resonance imaging. Plant Physiol **156:** 943–951

Valtaud C, Foyer CH, Fleurat-Lessard P, Bourbouloux A (2009) Systemic effects on leaf glutathione metabolism and defence protein expression caused by esca infection in grapevines. Funct Plant Biol **36:** 260

Valtaud C, Thibault F, Larignon P, Bertsch C, Fleurat-Lessard P, Bourbouloux A (2011) Systemic damage in leaf metabolism caused by esca infection in grapevines: Starch and soluble sugars in esca-infected *Vitis* leaves. Aust J Grape Wine Res **17:** 101–110

White C, Hallen F, Mostert L (2011) Symptoms and fungi associated with esca in South African vineyards. Phytopathol Mediterr **50:** 236–246

Yadeta KA, Thomma BPHJ (2013) The xylem as battleground for plant hosts and vascular wilt pathogens. Front Plant Sci **4:** 97

Zimmermann MH (1978) Vessel ends and the disruption of water flow in plants. Phytopathology **68:** 253–255

Zimmermann MH (1979) The discovery of tylose formation by a Viennese lady in 1845. IAWA Bull 51–56.

Zimmermann MH (1983) Xylem Structure and the Ascent of Sap. Springer-Verlag, Berlin